

# High-resolution Fly-over Beamforming Using a Small Practical Array

Jorgen Hald<sup>1</sup>

*Brüel & Kjaer SVM A/S, Naerum, DK-2850, Denmark*

Yutaka Ishii<sup>2</sup>

*Brüel & Kjaer Japan, Chiyoda-ku, 101-0048, Tokyo, Japan*

*and*

Tatsuya Ishii<sup>3</sup>, Hideshi Oinuma<sup>4</sup>, Kenichiro Nagai<sup>5</sup>, Yuzuru Yokokawa<sup>6</sup> and Kazuomi Yamamoto<sup>7</sup>  
*Japan Aerospace Exploration Agency (JAXA), Chofu, 182-8522, Tokyo, Japan*

The paper describes a commercially available fly-over beamforming system based on methodologies already published, but using an array that was designed for quick and precise deployment on a concrete runway rather than for minimum sidelobe level. Time domain tracking Delay And Sum (DAS) beamforming is the first processing step, followed by Deconvolution in the frequency domain to reduce sidelobes, enhance resolution, and get absolute scaling of the source maps. The system has been used for a series of fly-over measurements on a Business Jet type MU300 from Mitsubishi Heavy Industries. Results from a couple of these measurements are presented: Contribution spectra from selected areas on the aircraft to the sound pressure level at the array are compared against the total sound pressure spectrum measured by the array. One major aim of the paper is to verify that the system performs well although the array was designed with quick deployment as a main criterion. The results are very encouraging. A second aim is to elaborate on the handling of the array shading function in connection with the calculation of the Point Spread Function (PSF) used in deconvolution. Recent publications have used a simple formula to compensate for Doppler effects for the case of flat broadband spectra. A more correct formula is derived in the present paper, covering also a Doppler correction to be made in the shading function, when that function is used in the PSF calculation.

## Nomenclature

$b(t)$	=	DAS beamformed time signal
$B(\omega)$	=	DAS beamformed frequency spectrum
$B_{ij}(\omega)$	=	DAS beamformed spectrum at focus point $j$ due to model source $i$
$c$	=	Propagation speed of sound
DAS	=	Delay And Sum
$Df_{mi}, Df_{mj}$	=	Doppler frequency shift factor at microphone $m$ for signal from point $i$ and $j$ , respectively

---

<sup>1</sup> Senior Research Engineer, Innovations Group, Jorgen.Hald@bksv.com, AIAA Associate Member.

<sup>2</sup> Senior Application Engineer, Technology Service Department, Yutaka.Ishii@bksv.com.

<sup>3</sup> Associate Senior Researcher, Clean Engine Team, Aviation Program Group, ishii.tatsuya@jaxa.jp.

<sup>4</sup> Associate Senior Researcher, Clean Engine Team, Aviation Program Group, oinuma.hideshi@jaxa.jp.

<sup>5</sup> Associate Senior Researcher, Clean Engine Team, Aviation Program Group, nagai.kenichiro@jaxa.jp.

<sup>6</sup> Associate Senior Researcher, Civil Transport Team, Aviation Program Group, yokokawa.yuzuru@jaxa.jp, AIAA Senior Member.

<sup>7</sup> Senior Researcher, Civil Transport Team, Aviation Program Group, yamamoto.kazuomi@jaxa.jp, AIAA Senior Member.

$f$	= Frequency
$H_{ij}(\omega)$	= Element of Point Spread Function: From model source $i$ to focus point $j$
$i$	= Index of monopole point source in Deconvolution source model, $i = 1, 2, \dots, I$
$I$	= Number of focus/source points in calculation mesh
$j$	= Index of focus position, $j = 1, 2, \dots, I$ , or imaginary unit $\sqrt{-1}$
$k$	= Wavenumber ( $k = \omega/c$ )
$\kappa$	= Parameter defining steepness in radial cut-off of array shading filters
$m$	= Microphone index, $m = 1, 2, \dots, M$
$M$	= Number of microphones
$M_0$	= Mach number
$p_m(t)$	= Sound pressure time signal from microphone $m$
$\hat{p}_m(t)$	= Shaded time signal for microphone $m$
$P_m(\omega)$	= Frequency spectrum from microphone $m$
$P_{mi}(\omega)$	= Frequency spectrum from microphone $m$ due to model source $i$
PSF	= Point Spread Function (2D spatial power response to a monopole point source)
$\Pi_{\text{model}}$	= DAS beamformed pressure power (pressure squared) from the point source model in deconvolution
$\Pi_{\text{measured}}$	= DAS beamformed pressure power from an actual measurement
$Q_i(\omega)$	= Amplitude spectrum of model point source $i$
$r_{mj}(t)$	= Distance from microphone $m$ to moving focus point $j$
$r_{mj}$	= Distance from microphone $m$ to focus point $j$ at the center of an averaging interval
$R_m$	= Distance of microphone $m$ from array center
$R_{\text{coh}}(\omega)$	= Frequency dependent radius of active sub-array
$s_{mi}(t)$	= Distance from microphone $m$ to moving source point $i$
$s_{mi}$	= Distance from microphone $m$ to source point $i$ at the center of an averaging interval
$s_{0i}$	= Distance from array center to source point $i$ at the center of an averaging interval
$S_i(\omega)$	= Power spectrum of model point source $i$
$t$	= Time
$\mathbf{U}$	= Aircraft velocity vector
$U$	= Aircraft velocity, $U \equiv  \mathbf{U} $
$w_m(\tau)$	= Delay domain shading function applied to microphone $m$
$W_m(\omega)$	= Shading function in frequency domain
$\omega$	= Angular frequency ( $\omega = 2\pi f$ )

## I. Introduction

Beamforming has been widely used for noise source localization and quantification on aircrafts during fly-over for more than a decade<sup>1-6</sup>. The standard Delay And Sum (DAS) beamforming algorithm, however, suffers from poor low-frequency resolution, sidelobes producing ghost sources, and lack of absolute scaling. A special scaling method was introduced in Ref. 2 to get absolute contributions. During recent years, Deconvolution has been introduced as a post-processing step to scale the output contribution maps, but improving also both the low-frequency resolution and the sidelobe suppression<sup>3-8</sup>. For a planar distribution of incoherent monopole sources, which is a fairly good model for the aerodynamic noise sources of an aircraft, the output of a DAS beamforming at a given frequency will be approximately equal to the true source power distribution convolved in 2D with a frequency-dependent spatial impulse response, which is called the Point Spread Function (PSF). The PSF is defined entirely by the array geometry and the relative positioning of the array and the source plane, so for stationary sources it can be easily calculated and used in a deconvolution algorithm to estimate the underlying real source distribution. A difficulty with the use of deconvolution in connection with fly-over measurements is the fact that the DAS beamforming algorithm must be implemented in the time domain in order to track the aircraft, while deconvolution algorithms work only in frequency domain with the source at a fixed position relative to the array. Deconvolution in its basic form therefore cannot take Doppler shifts into account. A method to do that in an approximate and computationally efficient way was introduced in Ref. 3, further developed in Ref. 4 and applied with actual fly-over measurements in Ref. 5. The method adapts the PSF to the output from a DAS measurement on a moving point source, assuming flat broadband source spectra. Under that assumption the spectral shape will remain almost unchanged from the Doppler shifts. The method is able to compensate for the change in lobe pattern caused by Doppler shifts.

Most of the published applications of microphone arrays for fly-over measurement have been using rather large and complicated array geometries requiring considerable time to deploy and to measure the exact microphone positions. The present paper describes an investigation of the possibility of building an array system that can be quickly deployed on a runway and quickly taken down again. The entire system including the array and the implemented processing methodology will be described in section II, and its performance will be illustrated in section IV by results from a series of fly-over measurements on a business jet. The calculation of the PSF is treated in some detail. A derivation of the Doppler corrected PSF is given in the Appendix, and it turns out to have a slightly different form than assumed in References 3, 4 and 5, although it produces almost identical results when a frequency-independent array shading function is used. Section III presents an investigation of the match between the analytical frequency domain PSF and the DAS response to a moving point source.

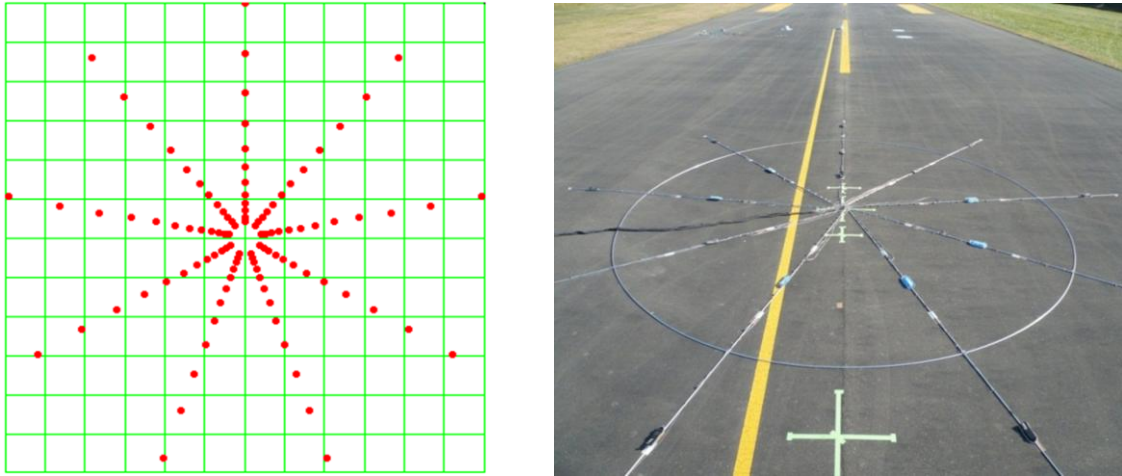


**Figure 1. Array geometry and picture of the array on the runway. Each microphone is clicked into position in the radial bars with the microphone tip touching the runway. “Half windscreens” can be added. The array diameter is 12 metres, and there are 9 radial line arrays each with 12 microphones.**

## II. Method and System Overview

The applied method follows the same overall measurement and processing scheme as the hybrid time-frequency approach described in Ref. 5. Aircraft position during a fly-over is measured with an onboard GPS system together with speed, Roll, Yaw and Pitch. Synchronization with array data is achieved through recording of an IRIG-B time-stamp signal together with the array data and also with the GPS data on the aircraft. The beamforming calculation is performed with a standard tracking time-domain DAS algorithm<sup>2</sup>. For each focus point in the moving system, FFT and averaging in short time intervals is then performed to obtain spectral noise source maps representing the aircraft positions at the middle of the averaging intervals. Diagonal Removal is implemented as described in Ref. 2, providing the capability of suppressing the contributions to the averaged spectra from the wind noise in the individual microphones. With sufficiently short averaging intervals, the array beam pattern will remain almost constant during the corresponding sweep of each focus point. This means that a deconvolution calculation can be performed for each FFT frequency line and for each averaging interval in order to enhance resolution, suppress sidelobes and scale the maps. Section II.B will elaborate on the compensation for Doppler effects in the calculation of the PSF used for the deconvolution.

Compensation for wind was not implemented in the proto-type software used for data processing. Fortunately there was almost no wind on the day when the measurements used in the present paper were taken. But the results to be presented in section IV reveal some small source offsets which could probably be reduced through a wind correction to be supported in released software. The proto-type software also does not support compensation for atmospheric losses. Such compensation will be needed to correctly reconstruct the source levels on the aircraft, but is not necessary to estimate the contributions from selected areas on the aircraft to the sound pressure at the array.

## A. Overall System Architecture

Fig. 1 shows the array geometry (left) and a picture of the array deployed on the runway. The array design and the use of a frequency dependent smooth array-shading function are inspired by Ref. 2. However, to support quick and precise deployment on the runway, a simpler star-shaped array geometry was implemented. The full array consists of 9 identical line-arrays which are joined together at a center plate and with equal angular spacing controlled by aluminium arcs. The 12 microphones on one line array of length 6 metres were clicked into an aluminium tube, which was rotated in such a way around its axis that the ¼ inch microphones were touching the runway. The surface geometry of that part of the runway, where the array was deployed, was very smooth and regular, so it could be characterized to a sufficient accuracy by just measuring a few slope parameters. Measurement of individual microphone coordinates therefore was not necessary: The vertical positions were automatically and accurately obtained from the known microphone coordinates in the horizontal plane and the runway slopes.

Due to the turbulence-induced loss of coherence over distance, a smooth shading function was used that focuses on a central sub-array, the radius of which is inversely proportional with frequency<sup>2</sup>. At high frequencies only a small central part of the array is therefore used, which must then have small microphone spacing. To counteract the resolution loss at low-to-medium frequencies resulting from the high microphone density at the center, an additional weighting factor was applied that ensured constant effective weight per unit area over the active part of the array<sup>2</sup>. The effective frequency-dependent shading to be applied to each microphone signal was implemented as a zero-phase FIR filter, which was applied to the signal before the beamforming calculation.

An important reason for the use of a shading function that cuts away signals from peripheral microphones at higher frequencies is to ensure that the PSF used for deconvolution will approximate the beamformer response to a point source measured under realistic conditions with air turbulence. The PSF is obtained purely from a mathematical model, so it will not be affected by air turbulence. If the PSF does not accurately model an actually measured point source response, then the deconvolution process cannot accurately estimate the underlying real source distribution that leads to the measured DAS map. The shading function must guarantee that at every frequency we use only a central part of the array which is not highly affected by air turbulence<sup>2</sup>.

A different way of handling the problem of a limited coherence diameter would be the use of nested arrays, where different sub-arrays are used in different frequency bands<sup>5</sup>. An advantage of the array design and shading method chosen in the present paper is the possibility of changing the shading function, and thus the active sub-array, continuously with frequency. As will be outlined below, Doppler correction must be applied in the shading filter, when that filter is used in the PSF calculation.

The array target frequency range was from 500 Hz to 5 kHz, and to support that a sampling rate of 16384 Samples/second was used. The microphones were B&K Type 4958 array microphones, and a B&K PULSE front-end was applied for the acquisition. In addition to the 108 array microphone signals, an IRIG-B signal and a line camera trigger signal were also recorded. While GPS data from the aircraft would be available through file transfer only after the measurement campaign, the line camera signal provided immediate information about aircraft passage time over the camera position within the time interval of the recorded microphone signals.

## B. Beamforming and Deconvolution Calculations

The implemented fly-over beamforming software supports two different kinds of output maps on the aircraft: Pressure Contribution Density and Sound Intensity. Both quantities can be integrated over selected areas on the aircraft to obtain the contributions from these areas to the sound pressure at the array and the radiated sound power, respectively. The present paper will be concerned only with the first quantity.

As argued above, the estimation of the Pressure Contribution Density does not require any compensation for losses during wave propagation in the atmosphere. For the same reason, Doppler amplitude correction is not required either. The first calculation step is to apply the shading filters  $W_m(\omega)$  to the measured microphone pressure signals  $p_m(t)$ ,  $m = 1, 2, \dots, M$  being an index over the  $M$  microphones,  $\omega$  the temporal angular frequency and  $t$  the time. To achieve equal weight per area over the active central sub-array the shading filters were defined as<sup>2</sup>:

$$W_m(\omega) = K(\omega) R_m^2 \left\{ 1 - \text{Erf} \left[ \kappa \left( \frac{R_m}{R_{\text{coh}}(\omega)} - 1 \right) \right] \right\}. \quad (1)$$

where  $R_m$  is the distance from microphone  $m$  to the array center, Erf is the Error Function,  $\kappa$  is a factor that controls the steepness of the radial cup-off,  $R_{\text{coh}}(\omega)$  is the assumed frequency dependent coherence radius (i.e. the radius of the active sub-array). Finally,  $K(\omega)$  is a scaling factor ensuring that at every frequency the sum of the microphone

weights equals one. The filters  $W_m(\omega)$  are applied to the microphone signals as a set of FIR filters. Effectively, the microphone signals are convolved by the impulse responses  $w_m(\tau)$  of the filters, providing the shaded microphone signals  $\hat{p}_m(t)$ :

$$\hat{p}_m(t) = (p_m \otimes w_m)(t). \quad (2)$$

For each point in the calculation mesh following the aircraft, DAS beamforming is then performed as:

$$b_j(t) = \sum_{m=1}^M \hat{p}_m \left( t + \frac{r_{mj}(t)}{c} \right), \quad (3)$$

$b_j(t)$  being the beamformed time signal at a focus point with index  $j$ ,  $c$  the propagation speed of sound, and  $r_{mj}(t)$  the distance from microphone  $m$  to the selected focus point at time  $t$ . Equation (3) must be calculated once for each desired sample of the beamformed signal, typically with the same sampling frequency as the measured microphone signals. With the applied rather low sampling rate in the acquisition, sample interpolation had to be performed on the microphone signals to accurately take into account the delays  $r_{mj}(t)/c$ . Equation (3) performs inherently a de-dopplerization providing the frequency content at the source<sup>2</sup>.

Once the beamformed time signals have been computed, averaging of Autopower spectra (using FFT) is performed for each focus point in time intervals that correspond to selected position intervals of the aircraft, typically of 10 m length. With a flight speed of 60 m/s, 256 samples FFT record length, 16384 Samples/second sampling rate, and 66.6% record overlap, the number of averages will be around 30. For the subsequent deconvolution calculation, an averaged spectrum is considered as belonging to a fixed position - the position of the focus point at the middle of the averaging time interval.

To introduce deconvolution and derive the associated PSF in a simple way, the case of non-moving source and focus points, i.e. with  $r_{mj}(t)$  equal to a constant distance  $r_{mj}$ , shall be considered first. Using  $e^{j\omega t}$  as the implicit complex time factor, Eq. (3) is then easily transformed to the frequency domain:

$$B_j(\omega) = \sum_{m=1}^M W_m(\omega) P_m(\omega) e^{jkr_{mj}}, \quad (4)$$

where  $B_j$  is the beamformed spectrum,  $W_m$  is the shading filter applied to microphone  $m$ ,  $P_m$  is the spectrum measured by microphone  $m$ , and  $k = \omega/c$  is the wavenumber.

Consider now a source model in terms of a set of  $I$  incoherent monopole point sources at each one of a grid of focus positions. Let  $i = 1, 2, \dots, I$  be an index over the sources and  $j = 1, 2, \dots, I$  an index over the focus point. The sound pressure at microphone  $m$  due to source  $i$  is then expressed in the following way:

$$P_{mi}(\omega) \equiv Q_i(\omega) s_{0i} \frac{e^{-jks_{mi}}}{s_{mi}} = Q_i(\omega) \frac{s_{0i}}{s_{mi}} e^{-jks_{mi}}, \quad (5)$$

where  $Q_i$  is the source amplitude,  $s_{mi}$  is the distance from microphone  $m$  to source number  $i$ , and  $s_{0i}$  is the distance from the center of the array to source number  $i$ . With this definition,  $Q_i$  is simply the amplitude of the sound pressure produced by source number  $i$  at the center of the array, which can be seen from Eq. (5) by considering the array center as microphone number 0. The beamformer output  $B_{ij}$  at position  $j$  due to source  $i$  is now obtained by use of Eq. (5) in Eq. (4):

$$B_{ij}(\omega) = \sum_{m=1}^M W_m(\omega) P_{mi}(\omega) e^{jkr_{mj}} = Q_i(\omega) \sum_{m=1}^M W_m(\omega) \frac{s_{0i}}{s_{mi}} e^{jk(r_{mj}-s_{mi})}. \quad (6)$$

Based on Eq. (6) we define the power transfer function  $H_{ij}(\omega)$  from source  $i$  to focus point  $j$  through the beamforming measurement and calculation process as follows:

$$H_{ij}(\omega) \equiv \left| \frac{B_{ij}(\omega)}{Q_i(\omega)} \right|^2 = \left| \sum_{m=1}^M W_m(\omega) \frac{S_{0i}}{S_{mi}} e^{jk(r_{mj}-s_{mi})} \right|^2. \quad (7)$$

Since the sources are assumed incoherent, they contribute additively to the power at focus position  $j$ , so defining the source power spectrum as  $S_i \equiv \frac{1}{2} |Q_i|^2$ , the total power represented by the source model at focus point  $j$  is:

$$\Pi_{\text{model},j}(\omega) = \sum_i H_{ij}(\omega) S_i(\omega). \quad (8)$$

Deconvolution algorithms aim at identifying the non-negative point source power values  $S_i$  of the model such that the modelled power at all focus points approximates as close as possible the power values  $\Pi_{\text{measured},j}$  obtained at the same points from use of the DAS beamformer Eq. (4) on the measured microphone pressure data:

$$\text{Solve } \Pi_{\text{measured},j}(\omega) = \sum_i H_{ij}(\omega) S_i(\omega) \quad \text{with } j=1,2,\dots,I, \quad S_i \geq 0. \quad (9)$$

The set of transfer functions  $H_{ij}(\omega)$  from a single source position  $i$  to all focus points  $j$  constitutes the PSF for that source position, describing the response of the beamformer to that point source:

$$\mathbf{PSF}_i(\omega) \equiv \{H_{ij}(\omega)\}_{j=1,2,\dots,I}. \quad (10)$$

Once Eq. (9) has been (approximately) solved by a deconvolution algorithm, the source strengths  $S_i$  represent the sound pressure power of the  $i$ 'th model source at the array center. The Pressure Contribution Density is therefore obtained just by dividing  $S_i$  by the area of the segment on the mapping plane represented by that monopole source.

Several deconvolution algorithms have been developed for use in connection with beamforming, see for example Ref. 7 for the DAMAS algorithm, introduced as the first one, and Ref. 8 for an overview. The DAMAS algorithm is computationally heavy, but supports arbitrary geometry of the focus/source grid, meaning that for a fly-over application an irregular area covering only the fuselage and the wings can be used<sup>4,5,8</sup>. Another advantage of DAMAS is that it can take into account the full variation of the PSF with source position  $i$ . Algorithms like DAMAS2 and FFT-NNLS are much faster, because they use 2D spatial FFT for the matrix-vector multiplications to be calculated during the deconvolution iteration. This, however, sets the restrictions that 1) the focus/source grid must be regular rectangular, and 2) the PSF must be assumed to be shift invariant to make the righthand side in Eq. (9) take the form of a convolution. The second requirement can be relaxed through the use of nested iterations<sup>8</sup>. All results of the present paper have been obtained using an FFT-NNLS algorithm based on a single PSF with source position at the center of the mapping area. No nested algorithm was used.

Having introduced the concepts related to deconvolution in connection with non-moving sources, we now return to the case of a moving source such as an aircraft. In that case the beamforming is performed in time domain using Eq. (3), followed by FFT and averaging in time intervals corresponding to selected position intervals of the aircraft. As a result we obtain for each averaging interval a set of beamformed FFT Autopower spectra  $\Pi_{\text{measured},j}$  covering all focus point indices  $j$ . Associating the spectra related to a specific averaging interval with the focus grid position at the middle of the averaging interval, one might as a first approximation just use the beamformed spectra in a stationary deconvolution based on Eq. (9), i.e. with the PSF calculated using Eq. (7). This would, however, not take into account the influence of Doppler shifts in the PSF calculation. The following modification was suggested and used in Ref. 4 and Ref. 5:

$$H_{ij}(\omega) = \left| \sum_{m=1}^M W_m \frac{S_{0i}}{S_{mi}} e^{jkDf_{mi}(r_{mj}-s_{mi})} \right|^2, \quad (11)$$

where  $Df_{mi}$  is the Doppler frequency shift factor of the signal from source  $i$  at microphone  $m$ :

$$Df_{mi} = \frac{1}{1 + M_0 \cos(\psi_{mi})}. \quad (12)$$

Here,  $M_0 \equiv |\mathbf{U}|/c$  is the Mach number,  $\mathbf{U}$  being the source velocity vector, and  $\psi_{mi}$  is the angle between the velocity vector  $\mathbf{U}$  and a vector from microphone  $m$  to point source number  $i$ . The inclusion of the Doppler shift factor in Eq. (11) changes to wavenumber  $k$  to the wavenumber  $Df_{mi}k = (Df_{mi}\omega)/c$  seen by microphone  $m$ .

During the testing of the beamforming software with simulated measurements, it turned out that the shading filter needs to be taken into account when doing Doppler corrections in the PSF calculation. Based on linear approximations in the calculation of distances, when the calculation grid is near the center of a selected averaging interval, it is shown in the Appendix that Eq. (6) should be replaced by:

$$B_{ij}(\omega) \equiv \sum_{m=1}^M W_m(\omega Df_{mj}) \frac{s_{0i}}{s_{mi}} \frac{Df_{mj}}{Df_{mi}} e^{jkDf_{mj}(r_{mj}-s_{mi})} Q_i\left(\omega \frac{Df_{mj}}{Df_{mi}}\right), \quad (13)$$

when processing data taken near the center of the interval. Here,  $Df_{mj}$  is the Doppler frequency shift factor at microphone  $m$  associated with a point source at focus position  $j$ . It is defined exactly as the factor for the source point  $i$ . Provided the source spectra  $Q_i(\omega)$  are very flat, the Doppler correction factor on the frequency in the argument of these spectra can be neglected, and Eq. (7) and (13) then lead to the following formula for the elements  $H_{ij}(\omega)$  of the PSF's:

$$H_{ij}(\omega) \equiv \left| \frac{B_{ij}(\omega)}{Q_i(\omega)} \right|^2 \equiv \left| \sum_{m=1}^M W_m(\omega Df_{mj}) \frac{s_{0i}}{s_{mi}} \frac{Df_{mj}}{Df_{mi}} e^{jkDf_{mj}(r_{mj}-s_{mi})} \right|^2. \quad (14)$$

One very important difference between Eq. (11) and Eq. (14) is the addition of the Doppler shift factor  $Df_{mj}$  on the frequency in the calculation of the array shading function  $W_m$ . The need for that factor comes from the fact that in the tracking DAS algorithm the shading filters are applied to the measured microphone signals, which include the Doppler shift, while the PSF is calculated in the moving system, where Doppler correction has been made. If the array shading functions  $W_m$  are very flat over frequency intervals of length equal to the maximum Doppler shift, the factors  $Df_{mj}$  are of course not needed. Another difference between Eq. (11) and Eq. (14) is that Eq. (14) has the focus point Doppler factor  $Df_{mj}$  in the exponential functions, whereas Eq. (11) uses the source point Doppler factor  $Df_{mi}$ . However, experience from simulated measurements have shown this difference to be of minor importance, since the two factors are very similar. The influence of the amplitude factor  $Df_{mj}/Df_{mi}$  is also negligible.

### III. Accuracy of the Point Spread Function

This section will investigate the agreement between the DAS response to a moving point source and a corresponding PSF calculated using Eq. (14). The geometry of the array described in section II.A was used, and the monopole point source was passing over at an altitude equal to 60 m with a speed of 60 m/s, which is representative for the real fly-over measurements to be described in section IV. A pseudo-random type of source signal, totally flat from 0 Hz to 6400 Hz, was used, consisting of 800 sine-waves of equal amplitude, but with random phases. With 16384 samples/s in the simulated measurement and an FFT record length equal to 256 samples, the FFT line width became 64 Hz, so the source signal had 8 frequency lines for each FFT line. FFT and averaging was performed over 10 m position intervals of the point source along the x-axis, so the averaging time was 1/6 of a second, which is comparable with the 1/8 second period length of the source signal. The FFT and averaging used a Hanning window and 66 % record overlap.

For the array shading, the radius  $R_{coh}(\omega)$  of the active central sub-array must be specified as a function of frequency,  $f$ . Reference 2 proposed the use of a radius inversely proportional with frequency:

$$R_{coh}(f) = \frac{f_{1\text{metre}}}{f} \cdot 1 \text{ m}, \quad (15)$$

$f_{1 \text{ metre}}$  being the frequency with 1 metre radius of the central coherent area. Based on actual measurements, a value around 4 kHz was proposed<sup>2</sup>. The actual measurements presented in the present paper were taken on a day with almost no wind, and we have found a value of  $f_{1 \text{ metre}}$  equal to 6 kHz to provide good results, so that value has been used also in the simulated measurements.

After shading, DAS beamforming was performed at a grid of 61 x 61 points with 0.25 m spacing, covering an area of 15 m x 15 m with the point source at the center. The PSF was then calculated across the same grid of points, for a source also at the center. Diagonal Removal was not applied.

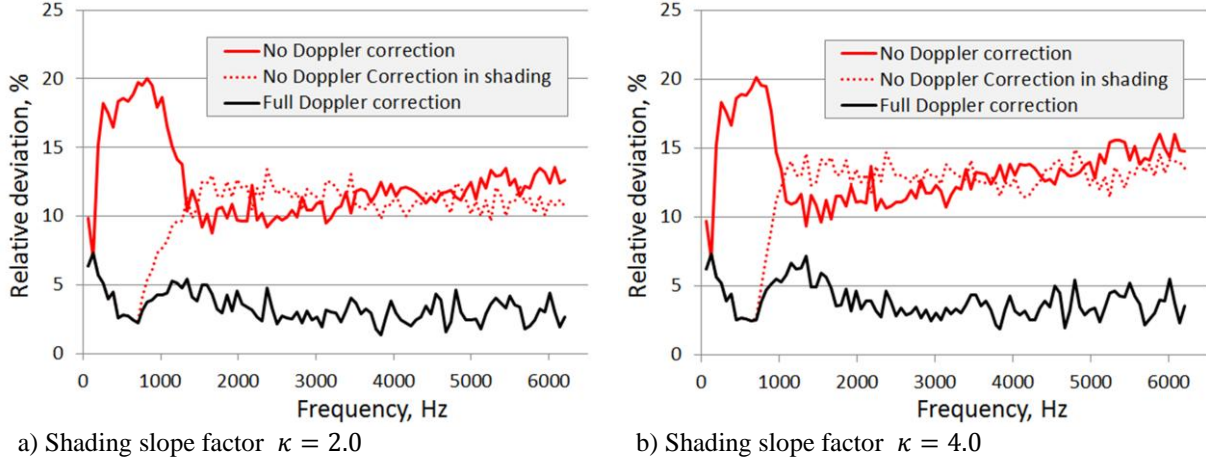


**Figure 2. Relative average deviation between PSF and DAS over a 15 m x 15 m area centered at  $x = -30$  m.**

Figure 2 shows as a function of frequency the average relative deviation between the two maps calculated as:

$$\text{Relative Deviation} = \frac{\sqrt{\sum_j (H_{ij} - \Pi_{\text{measured},j})^2}}{\sqrt{\sum_j (\Pi_{\text{measured},j})^2}} \cdot 100\% , \quad (16)$$

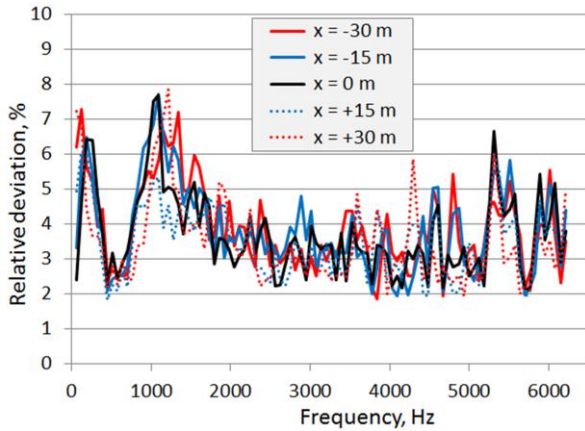


**Figure 3. Relative average deviation between PSF and DAS over a 15 m x 15 m area centered at a set of different  $x$ -coordinates.  $\kappa = 4.0$ .**

where the PSF source position  $i$  is at the center of the area, and  $\Pi_{\text{measured},j}$  is from a simulated measurement on that source with unit amplitude. The left part a) shows the result for a rather smooth radial cut-off in the shading function,  $\kappa = 2.0$ , while in the righthand part b) a medium steep cut-off  $\kappa = 4.0$  was used. In both cases, three levels of Doppler correction was used in the calculation of the PSF: The full red curve represents the case of no Doppler correction made, meaning that the PSF was calculated from Eq. (7). For the dotted red curve Eq. (14) was used, but without the Doppler shift factor in the shading function  $W_m$ . The result is almost identical with what would be obtained using Eq. (11). The full black spectrum is obtained using Eq. (14). Clearly, use of the Doppler factor in the calculation of the shading function is needed. The remaining error was highly depending on the applied signal and the averaging time, and no other important influencing factors were identified. So this residual error seems to be caused by the very short averaging performed in the tracking DAS beamformer. The change in shape of the deviation spectra around 800 Hz occurs where the radial cut-off of the shading function sets in.

Figure 3 shows the deviation achieved through use of Eq. (14) for PSF calculation at a set of  $x$ -coordinates. The deviation is seen to have approximately the same level independent of position during the simulated fly-over, when Eq. (14) is used for calculation of the PSF.

#### IV. Application to MU300 Business-jet Fly-over

The system was applied as a part of a fly-over test campaign in November 2010 at Taiki Aerospace Research Field (Taiki, Hokkaido, Japan) under a Joint research work between JAXA and B&K. JAXA was conducting the test campaign, where fly-over noise source localization technologies, including their own acoustic array, were developed. Around 120 measurements were taken on an MU300 business jet from Mitsubishi Heavy Industries. Figure 5 contains a picture of the MU300 aircraft, which has overall length and width equal to 14.8 m and 13.3 m, respectively. It has two jet engines on the body, just behind and over the wings. The nose of the aircraft is used as the reference in the position information obtained from the onboard GPS system. As indicated in Fig. 4, the center of the global coordinate system is on the runway at the center of the array.

The approach adopted for time-alignment of array recordings and aircraft position information from the aircraft was described in section II.A. The data file from the on-board GPS based positioning system provided with 5 metre interval along the runway the following information:

- Very accurate absolute time from the IRIG-B system.
- 3 position coordinates with accuracy between 5 cm and 30 cm.
- 3 speed coordinates with accuracy around 0.005 m/s.
- Roll, Pitch and Yaw with approximate accuracy  $0.005^\circ$ .

This information in combination with the IRIG-B signal recorded with the microphone signals was used in all data processing for accurate reconstruction of the aircraft position at every sample of the microphone signals.

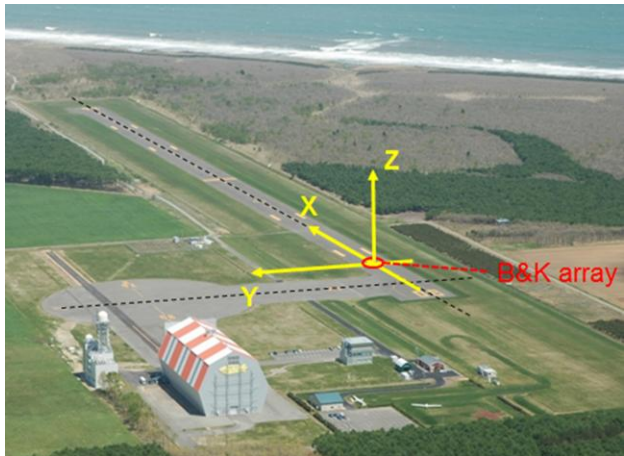
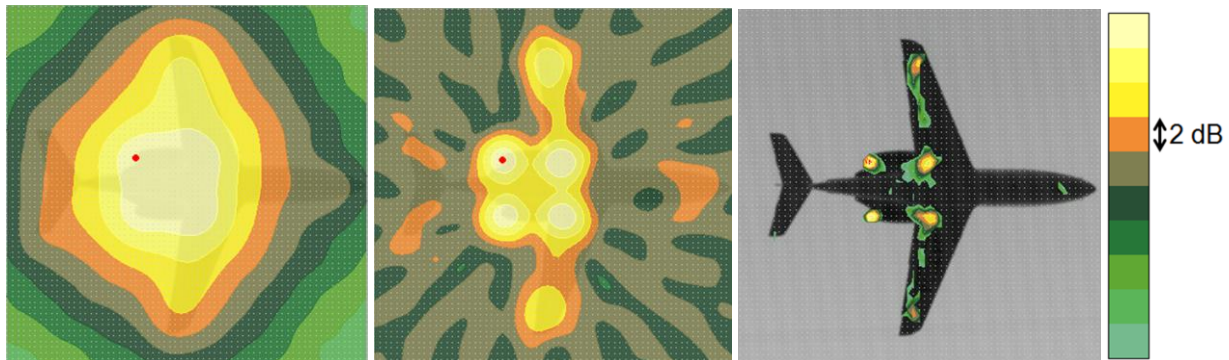


Figure 4. Taiki Aerospace Research Field with indication of array position and global coordinate system.



Figure 5. Picture of the MU300 business jet.



a) DAS, no shading, no diag. rem.

b) DAS, shading, no diag. rem.

c) DAS + NNLS, shading, diag. rem.

Figure 6. Illustration of the improvements in resolution and dynamic range obtained through the use of shading and deconvolution. The data are from a level flight with engine idle and the aircraft in landing configuration. The display dynamic range is 20 dB, corresponding to 2 dB contour interval.

### A. Illustration of processing steps

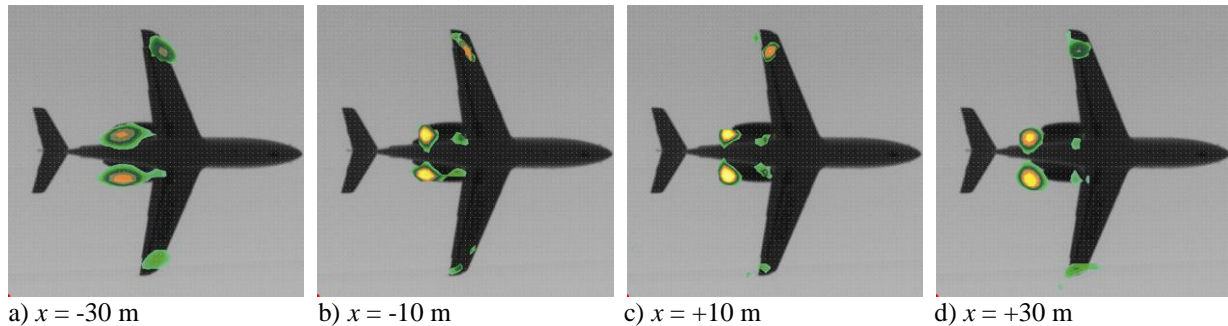
The purpose of this section is just to illustrate the huge improvement in resolution and dynamic range that is achieved through the combination of shading and deconvolution. For this illustration a *level flight* was chosen with *engine idle* and the aircraft in *landing configuration*. Altitude was 59 m, and the speed was 57 m/s.

Figure 6 shows results for the 1 kHz octave band, averaged over a 15 m interval centered where the nose of the aircraft is 5 m past the array center, i.e. at  $x = 5$  m. The resulting FFT spectra were synthesized into full octave bands. The displayed dynamic range is 20 dB, corresponding to 2 dB level difference between the colours. Plot a) shows the DAS map obtained without shading, meaning that resolution will be poor due to the concentration of microphones near the array center. Use of the shading function improves resolution considerably, as seen in plot b), but it also amplifies the sidelobes due to the large microphone spacing across the outer part of the active sub-array, where each microphone is also given a large weight. Fortunately, the deconvolution process is able to significantly reduce these sidelobes as can be seen in plot c). Better sidelobe suppression could have been achieved in DAS by the use of more optimized irregular array geometries (e.g. multi spiral), but in the present work the focus has been on the ease of array deployment, and deconvolution seems to compensate quite well.

All maps were calculated using a 16 m x 16 m grid with 0.25 m spacing, leading to  $65 \times 65 = 4225$  calculation points. In the following, 10 m averaging intervals will be always used. The total calculation time for 7 intervals, including DAS and FFT-NNLS calculations, was approximately 5 min on a standard Dell Latitude E6420 PC.

### B. Contour plots of Pressure Contribution Density

The results to be presented in this section and in the subsequent section IV.C are all from a *level flight* at 63 m altitude, with 61 m/s speed, *engine idle*, and with the aircraft in *clean configuration*. All results were obtained using shading, diagonal removal and FFT-NNLS deconvolution based on a PSF with full Doppler correction as described in Eq. (14).



**Figure 7. Pressure Contribution Density plots for the 1 kHz octave at 4 positions during a *level flight* with *engine idle* and the aircraft in *clean configuration*. The averaging intervals were 10 m long and centered at the listed positions. The 20 dB colour scale from Fig. 6 is reused. Threshold is constant across the four maps with full dynamic range used at  $x = +10$  m, where the engine nozzles are exactly over the array center.**

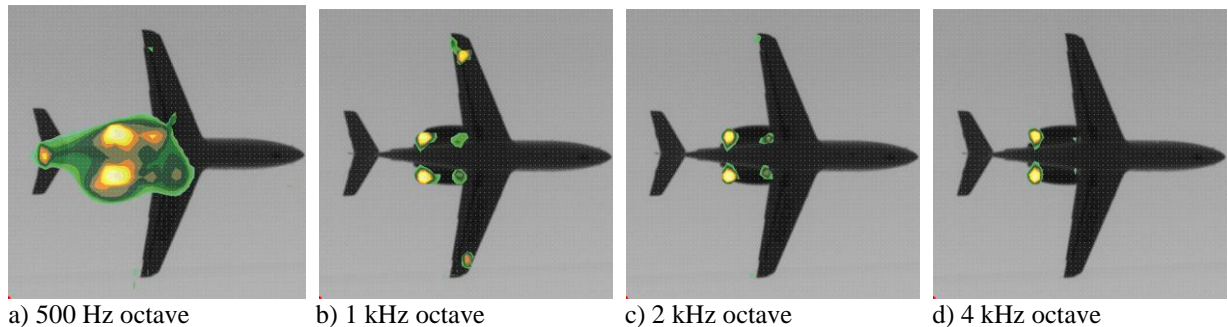


**Figure 8. Octave band Pressure Contribution Density maps for the averaging interval at  $x = 0$ . Again, the 20 dB colour scale from Fig. 6 is reused. For each map the threshold is adjusted to show a 20 dB range.**

Figure 7 contains contour plots of the Pressure Contribution Density for the 1 kHz octave band when the nose of the aircraft is at  $x = -30, -10, 10$  and  $30$  m. A 20 dB fixed display range has been used to reveal source level changes during the fly-over. At  $x = +10$  m the engine nozzles are almost exactly over the center of the array. The

strong nozzle sources are seen to shift a bit in the  $x$ -direction as the aircraft moves past the array. This is at least partially because the engine is at a slightly higher altitude than the mapping plane, which is at the level of the aircraft nose, see Fig. 5. Based on aircraft geometry, the nozzle sources should shift approximately 1/3 of the engine length due to that phenomenon when the aircraft moves from  $x = -30$  m to  $x = +30$  m. The two weaker source in front of the nozzles are probably the intakes, which are only partially visible from the array because of the wings. Close to the wing tips two more significant sources are seen in this 1 kHz octave band. Probably these sources are the openings of two drain tubes or small holes and gaps. The narrowband spectral results to be presented in the following section IV.C show that these two sources are narrowbanded and concentrated near 1 kHz.

Figure 8 contains contour plots similar to those of Fig. 7, but with the nose of the aircraft at  $x = 0$  m and covering the octave bands from 500 Hz to 4 kHz. Clearly, the two sources some small distance from the wing tips exist only within the 1 kHz octave band. The 500 Hz octave includes frequencies well below 500 Hz, where the array is too small to make deconvolution work effectively, so here resolution is poor. Notice that the system provides almost constant resolution across a fairly wide frequency range. This is true also for the DAS maps, i.e. without deconvolution, the explanation being that the diameter of the active sub-array is inverse proportional with frequency above 1 kHz.

### C. Pressure Contribution Spectra at the Center of the Array

As mentioned in section II.B, the Pressure Contribution Density maps - such as those in Fig. 7 - can be area integrated to give estimates of the contributions from selected areas to the sound pressure at the center of the array. As a reference for these contributions, and for validation purposes, it is desirable to compare them with the pressure measured directly at the array. Since there was no microphone at the array center, the average pressure power across all microphones was used. The directly measured spectra, however, contain Doppler shifts, whereas the area-integrated spectra are based on maps of de-dopplerized data. To compare the spectral contents, the Doppler shift status must be brought into line for the two spectra. Since it is natural to have the Doppler shift included, when dealing with the noise at the array, a choice was made to “re-dopplerize” the Pressure Contribution Density maps on the aircraft. So this was actually done also for the maps in Fig. 7 and Fig. 8.

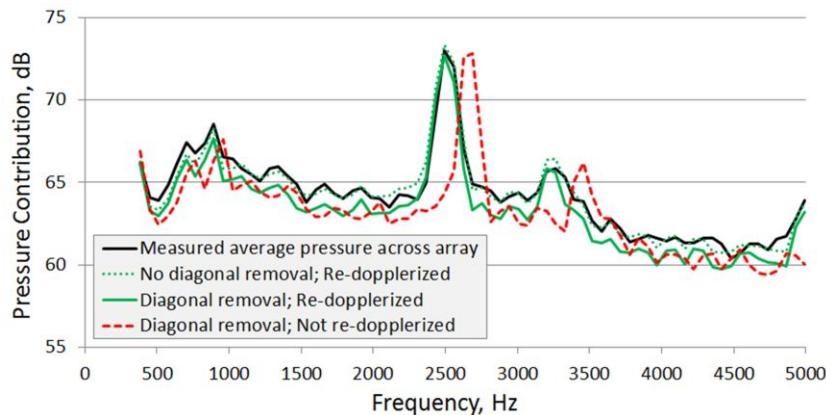


**Figure 9. Measured average pressure spectrum compared with pressure contributions calculated by integrating over the full mapping area seen in Fig. 7d.**

Without Diagonal Removal, the level of the calculated contribution spectrum matches very well with the measured array pressure. Diagonal removal leads to a small under-estimation amounting to approximately 1 dB, part of which is flow noise in the individual microphones.

In the derivation of the PSF in Eq. (14) we had to assume a flat spectrum to proceed from Eq. (13). Clearly, the spectrum in Fig. 9 is not flat around the narrow peak at 2.5 kHz. Eq. (14) was used anyway across the full frequency range, and the spectral peaks seem well reproduced. But to ensure an accurate handling of Doppler effects around sharp spectral peaks (tones) in deconvolution, a special handling should be implemented modeling the energy flow between frequency lines<sup>4</sup>. This becomes an important issue, if the level difference between a peak and the surrounding broadband spectrum approaches or even exceeds the dynamic range (sidelobe suppression) of the array with DAS beamforming. This is not the case here, but close.

The full black curve in Fig. 9 represents the directly measured array pressure spectrum based on FFT's with 256 samples record length, Hanning window, and averaging over a time interval corresponding to that used at the aircraft, but delayed with the sound propagation time from the aircraft to the array. The three pressure contribution spectra in the same figure were integrated over the full mapping area for the averaging interval at  $x = +30$  m, represented also in Fig. 7d. As expected, the re-dopplerization shifts downwards the spectral peaks in the contribution spectra to match very

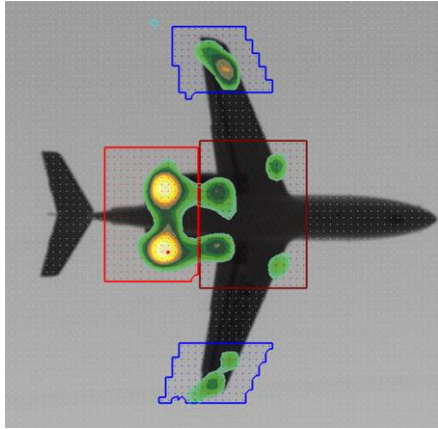


**Figure 10. Sub-areas used for integration of pressure contribution. The sources at the inner front edge of the wings are probably two fins.**

By integrating the Pressure Contribution Density over only partial areas, one can estimate the contribution from these areas to the sound pressure at the array. Figure 10 shows a set of sub-areas to be considered beyond the full mapping area: 1) The engine nozzles. 2) The central area, covering engine intake, wheel wells, and the inner part of the wings. 3) The outer approximately 1/3 of both wings. The colours of the areas will be re-used in the contribution spectra.

Figure 11 contains the contribution spectra for the same aircraft positions as represented by the contour maps in Fig. 7. In the present *clean* configuration of the aircraft, the engine nozzles are seen to have by far the dominating noise contribution, even though the engine is in idle condition. A small exception is a narrow frequency band near 1 kHz, where the sources near the wing tip are dominating. Except for very few exceptions, the full area contribution is within 1 dB from the measured average sound pressure over the array. Part of this difference is due to flow noise in the individual microphones. So the underestimation on the full-area contribution due to the use of diagonal removal is very small, but may cause low-level secondary sources in Fig. 7 and 8 to become invisible. The shown 30 dB of dynamic range in the spectra of Fig. 11 is probably a bit too large to say that all visible details are “real”.

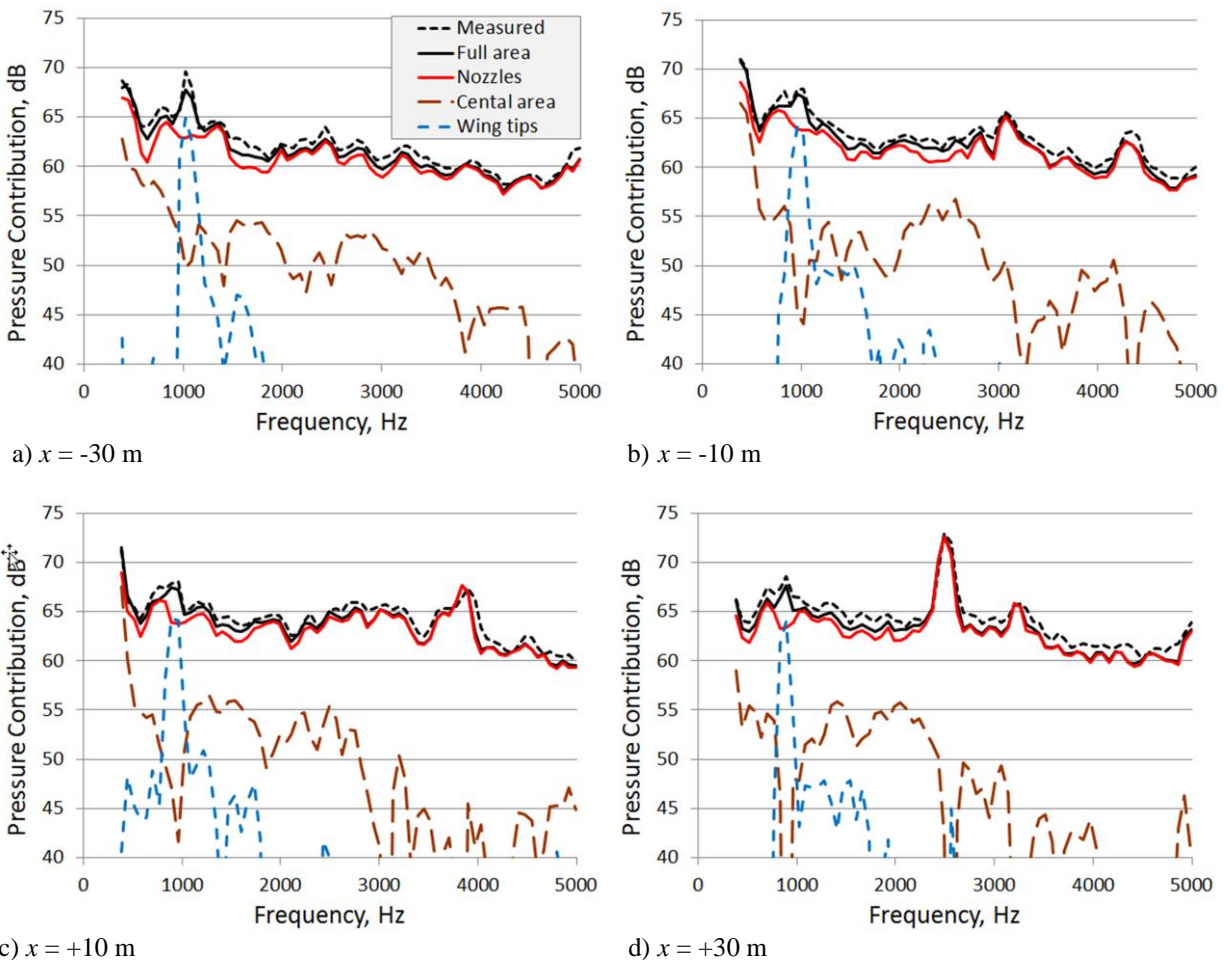


**Figure 11. Pressure contributions from the areas of Fig. 10 to the sound pressure at the array center.**

## V. Conclusion

The paper has described a system and a methodology for performing high resolution fly-over beamforming using an array designed for fast and precise deployment on a runway. Due to this requirement, a rather simple array geometry not optimized for best sidelobe suppression was used. Our hope was that the use of deconvolution could compensate for that. The system was designed to cover the frequency range from 500 Hz to 5 kHz, and it proved to provide very good resolution and dynamic range across these frequencies, except perhaps just around 500 Hz. Results have been presented in the paper from a couple of measurements out of approximately 120 recordings taken on an MU300 business jet at Taiki Aerospace Research Field, Taiki, Hokkaido, Japan, in November 2010. The results are very encouraging.

A special focus has been on the use of an array shading function that changes continuously with frequency, and in particular on the implications of that in connection with deconvolution. It was shown that Doppler shifts have to be taken into account in the use of the shading function in connection with calculation of the Point Spread Function used for deconvolution.

## Appendix

The present Appendix presents a derivation of Eq. (13). We consider an arbitrarily selected averaging interval, and we choose also arbitrarily a single model point source with index  $i$ . For convenience we measure time relative to the center of the selected averaging interval.

The first problem is to derive a linear approximation for the time  $t_m$  where the source signal radiated at time  $t_s$  reaches microphone  $m$ , valid for  $|t_s| \ll 1$ . To do that, the distance from point source  $i$  to microphone  $m$  is approximated as:

$$s_{mi}(t_s) \cong s_{mi} + \cos(\psi_{mi})Ut_s \quad \text{for } |t_s| \ll 1, \quad (17)$$

where  $U \equiv |\mathbf{U}|$  is the aircraft speed, and  $\psi_{mi}$  is the angle between the velocity vector  $\mathbf{U}$  and a vector from microphone  $m$  to the point source, both at the center of the averaging interval. In the same way we get for the distance from focus point  $j$  to the microphone:

$$r_{mj}(t) \cong r_{mj} + \cos(\psi_{mj})Ut \quad \text{for } |t| \ll 1. \quad (18)$$

The signal radiated at time  $t_s$  arrives at microphone  $m$  at time  $t_m$  given as:

$$t_m = t_s + \frac{s_{mi}(t_s)}{c}. \quad (19)$$

Using Eq. (17) and the expression in Eq. (12) for the Doppler shift factor, we can rewrite Eq. (19) as:

$$t_m \cong \frac{s_{mi}}{c} + \frac{t_s}{Df_{mi}}. \quad (20)$$

This equation is easily solved for  $t_s$  with the result:

$$t_s \cong Df_{mi} \cdot \left( t_m - \frac{s_{mi}}{c} \right), \quad (21)$$

which is then valid for  $\left| t_m - \frac{s_{mi}}{c} \right| \ll 1$ .

For the microphone signals from point source  $i$  we need an expression equivalent with Eq. (5), just in time domain and for the moving source. As argued in section II.B, the Doppler amplitude factor can be neglected, when estimating Pressure Contributions. Doing that, the microphone pressure gets the following simple form<sup>5</sup>:

$$p_{mi} \left( t_s + \frac{s_{mi}(t_s)}{c} \right) = s_{oi} \frac{q_i(t_s)}{s_{mi}(t_s)}, \quad (22)$$

containing the propagation delay  $s_{mi}(t_s)/c$  and the inverse distance decay in connection with the source signal  $q_i$ . In Eq. (22) we approximate the time-varying inverse distance decay by its value for  $t_s = 0$ , and we use the delay approximation of Eq. (21):

$$p_{mi}(t_m) \cong \frac{s_{oi}}{s_{mi}} q_i \left( Df_{mi} \cdot \left( t_m - \frac{s_{mi}}{c} \right) \right) \quad \text{for} \quad \left| t_m - \frac{s_{mi}}{c} \right| \ll 1. \quad (23)$$

The first step in the DAS calculation is application of the individual shading filters to the microphone signals. In time domain this can be expressed as convolution with the impulse responses  $w_m(\tau)$  of these filters, see Eq. (2):

$$\begin{aligned} \hat{p}_{mi}(t_m) &= (p_{mi} \otimes w_m)(t_m) = \int_{-\infty}^{\infty} p_{mi}(\tau) w_m(t_m - \tau) d\tau \\ &\cong \frac{s_{oi}}{s_{mi}} \int_{-\infty}^{\infty} q_i \left( Df_{mi} \cdot \left( \tau - \frac{s_{mi}}{c} \right) \right) w_m(t_m - \tau) d\tau \end{aligned} \quad (24)$$

Here the approximation of Eq. (23) has been inserted. An apparent conflict in this context is the integral going from  $-\infty$  to  $+\infty$  while at the same time we use an approximation valid for only small values of the integration variable. Both here and in the later Fourier integrals we have to think of using windowed source signals, meaning that the integrals will have contributions only from time segments close to time zero.

The shaded microphone signals are now used in DAS beamforming as expressed in Eq. (3):

$$b_{ij}(t) = \sum_{m=1}^M \hat{p}_{mi} \left( t + \frac{r_{mj}(t)}{c} \right). \quad (25)$$

To proceed, we need to use the linear approximation of Eq. (18) for the distances  $r_{mj}(t)$  between microphones and focus points. As a result we obtain an approximation similar to the one in Eq. (20):

$$t + \frac{r_{mj}(t)}{c} \cong \frac{r_{mj}}{c} + \frac{t}{Df_{mj}} \quad \text{for} \quad |t| \ll 1. \quad (26)$$

Use of Eqs. (26) and (24) in Eq. (25) leads to:

$$\begin{aligned} b_{ij}(t) &= \sum_{m=1}^M \hat{p}_{mi} \left( t + \frac{r_{mj}(t)}{c} \right) \cong \sum_{m=1}^M \hat{p}_{mi} \left( \frac{r_{mj}}{c} + \frac{t}{Df_{mj}} \right) \\ &\cong \sum_{m=1}^M \frac{s_{oi}}{s_{mi}} \int_{-\infty}^{\infty} q_i \left( Df_{mi} \cdot \left( \tau - \frac{s_{mi}}{c} \right) \right) w_m \left( \frac{r_{mj}}{c} + \frac{t}{Df_{mj}} - \tau \right) d\tau \end{aligned} \quad (27)$$

The final step to obtain the frequency domain response  $B_{ij}(\omega)$  is to Fourier transform the signal  $b_{ij}(t)$ . To do that we notice first that in Eq. (27) the time variable  $t$  occurs only in the argument of the shading impulse response function  $w_m$ . The argument of  $w_m$  has the form of a linear function of  $t$ . To work out the Fourier integral of  $b_{ij}(t)$  we therefore need the following formula:

$$\int_{-\infty}^{+\infty} w(at+b) e^{-j\alpha\omega t} dt = a^{-1} e^{j\omega \frac{\alpha b}{a}} W\left(\frac{\alpha}{a}\omega\right), \quad (28)$$

with  $\alpha = 1$ ,  $a = (Df_{mj})^{-1}$ , and  $b = \frac{r_{mj}}{c} - \tau$ .  $W$  is the Fourier transform of  $w$ . Eq. (28) can be easily verified by substituting a new variable for  $(at+b)$  in the integral. From use of Eq. (28) in Eq. (27) we get:

$$\begin{aligned} B_{ij}(\omega) &\equiv \int_{-\infty}^{+\infty} b_{ij}(t) e^{-j\omega t} dt \\ &\cong \sum_{m=1}^M \frac{s_{oi}}{s_{mi}} \int_{-\infty}^{\infty} q_i \left( Df_{mi} \cdot \left( \tau - \frac{s_{mi}}{c} \right) \right) Df_{mj} e^{jDf_{mj}\omega \left( \frac{r_{mj}}{c} - \tau \right)} W_m(Df_{mj}\omega) d\tau, \quad (29) \\ &= \sum_{m=1}^M W_m(Df_{mj}\omega) \frac{s_{oi}}{s_{mi}} Df_{mj} e^{jDf_{mj}\omega \frac{r_{mj}}{c}} \int_{-\infty}^{\infty} q_i \left( Df_{mi} \cdot \left( \tau - \frac{s_{mi}}{c} \right) \right) e^{-jDf_{mj}\omega \tau} d\tau \end{aligned}$$

where the factors are just re-arranged in the last line. The remaining integral in Eq. (29) has also the form of Eq. (28), only with  $\alpha = DF_{mj}$ ,  $a = Df_{mi}$ , and  $b = -Df_{mi} \frac{s_{mi}}{c}$ . Use of Eq. (28) with these parameter values in Eq. (29) leads to:

$$\begin{aligned} B_{ij}(\omega) &\cong \sum_{m=1}^M W_m(Df_{mj}\omega) \frac{s_{oi}}{s_{mi}} Df_{mj} e^{jDf_{mj}\omega \frac{r_{mj}}{c}} \frac{1}{Df_{mi}} e^{j\omega \left( -Df_{mi} \frac{s_{mi}}{c} \right)} Q_i \left( \frac{Df_{mj}}{Df_{mi}} \omega \right) \\ &= \sum_{m=1}^M W_m(Df_{mj}\omega) \frac{s_{oi}}{s_{mi}} \frac{Df_{mj}}{Df_{mi}} e^{jDf_{mj}\omega \left( \frac{r_{mj}}{c} - \frac{s_{mi}}{c} \right)} Q_i \left( \frac{Df_{mj}}{Df_{mi}} \omega \right) \end{aligned} \quad (30)$$

which is the expression given in Eq. (13). Q.e.d.

### Acknowledgments

The authors would like to thank Diamond Air Service Incorporation for their support in conducting the fly-over tests.

### References

- <sup>1</sup>Michel, U., Barsikow, B., Helbig, J., Hellmig, M., and Schüttpelz, M., "Flyover Noise Measurements on Landing Aircraft with a Microphone Array," AIAA Paper 98-2336.
- <sup>2</sup>Sijtsma, P. and Stoker, R., "Determination of Absolute Contributions of Aircraft Noise Components Using Fly-over Array Measurements," AIAA Paper 2004-2958.
- <sup>3</sup>Guérin, S., Weckmüller, C., and Michel, U., "Beamforming and Deconvolution for Aerodynamic Sound Sources in Motion," Berlin Beamforming Conference (BeBeC) 2006, Paper BeBeC-2006-16.
- <sup>4</sup>Guérin, S., and Weckmüller, C., "Frequency Domain Reconstruction of the Point-spread Function for Moving Sources," Berlin Beamforming Conference (BeBeC) 2008, Paper BeBeC-2008-14.
- <sup>5</sup>Guérin, S. and Siller, H., "A Hybrid Time-Frequency Approach for the Noise Localization Analysis of Aircraft Fly-overs," AIAA Paper 2008-2955.
- <sup>6</sup>Siller, H., Drescher, M., Saueressig, G., and Lange, R., "Fly-over Source Localization on a Boeing 747-400," Berlin Beamforming Conference (BeBeC) 2010, Paper BeBeC-2010-13.
- <sup>7</sup>Brooks, T.F., Humphreys, W.M., "A Deconvolution Approach for the Mapping of Acoustic Sources (DAMAS) Determined from Phased Microphone Arrays," AIAA Paper 2004-2954.
- <sup>8</sup>Ehrenfried, K. and Koop, L., "A comparison of iterative deconvolution algorithms for the mapping of acoustic sources," AIAA Paper 2006-2711.